1. Łukasz MACIURA[1], 2. Tomasz RYMARCZYK[1,2], 3. Dariusz WÓJCIK[1,2]
4. Konrad GAUDA[2], 5. Marcin KOWALSKI[2]

Netrix S.A., Research & Development Centre, Lublin, Poland (1),
WSEI University, Lublin, Poland (2)
ORCID: 1. 0000-0001-8657-3472; 2. 0000-0002-4200-3432; 3. 0000-0002-3524-9151; 4. 0000-0002-7300-6978; 5. 0000-0002-1644-0612

doi:10.15199/48.2023.06.27

Deep learning correction for image reconstruction in electrical impedance tomography using UNet model

***Abstract**. This article was inspired by a similar Deep DBar algorithm, where a modified UNet convolutional model was used to correct the output of the DBar algorithm using the UNet model. However, instead of the DBar algorithm, another deterministic electrical impedance tomography reconstruction algorithm was used in this solution. The modified UNet model was used to successfully correct the initial reconstructions, which were computed using Kotre regularities using pseudo-inversion of the sensitivity matrix.*

***Streszczenie.** Ten artykuł został inspirowany podobnym algorytmem Deep DBar, w którym zmodyfikowany model splotowy UNet został użyty do skorygowania danych wyjściowych algorytmu DBar przy użyciu modelu UNet. Jednak zamiast algorytmu DBar w tym rozwiązaniu zastosowano inny deterministyczny algorytm rekonstrukcji elektrycznej tomografii impedancyjnej. Zmodyfikowany model UNet został wykorzystany do skutecznej korekcji wstępnych rekonstrukcji, które zostały obliczone przy użyciu regularności Kotrego z wykorzystaniem pseudo-inwersji macierzy czułości (**Poprawa rekonstrukcji tomografii impedancyjnej oparta o głębokie uczenie przy użyciu modelu UNet**).*

Keywords: Electrical Impedance Tomography, convolutional neural networks, *UNet*.
Słowa kluczowe: elektryczna tomografia impedancyjna, sieci konwolucyjne, *UNet*.

Introduction

Electrical Impedance Tomography (EIT) reconstruction is a difficult (undetermined) problem to resolve. It relies on the reconstruction of the image on the scene based on a vector obtained from numerous measurements using *EIT* sensors. There are a lot of *EIT* reconstruction algorithms available in the bibliography. On the other hand, the most excellent results are obtained using neural networks (profound learning solutions).

Various numerical methods are available for such tasks [1-25]. The research [1] used logistic regression using an elastic net to reconstruct *EIT*. The research [2] uses Artificial Neural Networks to reconstruct the image. This article describes using separate neural networks for each output pixel to reconstruct individual pixels. It produces better results than a single *NN* with multiple outputs, but the amount of neural networks and parameters in each network is huge. The article [17] showed the example application of convolutional neural network in EIT reconstruction.

Nowadays, the multiple *ANN EIT* reconstruction methods are based on deep and convolutional autoencoders. Paper [16] describes a solution based on *EIT* reconstruction gained using a deterministic algorithm (*D-Bar*) and applies *UNet* convolutional model to correct these initial reconstructions. The images are the input and output of *the UNet model, so* we can use them to correct other reconstruction algorithms' results.

Another method using deep autoencoders described in [20] reconstructs lungs object based on Electrical Impedance Tomography. The method includes three steps:

1) A deep convolutional autoencoder is trained on reference (output) images (the lungs image reconstruction problem is presented in the paper).
2) The images encoded by the encoder part from the convolutional autoencoder trained in the previous step are applied as outputs to train of network with fully connected layers to predict such vectors based on electric potential vectors obtained from *EIT* sensors.
3) In the last stage, the joint model of both pre-trained networks is prepared. Finally, the output from the pre-trained model in stage 2 is inserted into the encoder part from the autoencoder obtained in the initial stage. This resultant hybrid network can reconstruct *EIT* images based on electrical potentials from Electrical Impedance Tomography measurements.

The research presented in this article was inspired by the algorithm called *Deep DBar* [16], which relies on the improvement of deterministic *DBar* algorithm output [24] using deep learning using the *UNet* model [26] with modifications. After examination of the *DBar* algorithm, it turned out that it has a relatively very low speed, so another faster deterministic algorithm for some practical applications should be developed. After examination of various models, there are also available different *DNN* models useful for *EIT* reconstruction using autoencoders [22], [23]. This model contains two separately trained parts (*SAE* and *LR*). The coder part from pre-trained earlier *SAE* autoencoder encodes potential vector and logistic regression layers (*LR*) reconstructing *EIT* images. The training process of the *SAE* autoencoder includes a few repeatable stages. All stages are used to train the *SAE* model to encode *EIT* potential vectors; thus, the potential vectors are on the input and output in this model. Initially, the *SAE* autoencoder contains only three layers (input layer, hidden layer and output layer). The hidden layer contains the encoded vector from the first step (which will be used in the next step). After a few iterations of that process, a deep autoencoder with more hidden layers to encode potential vectors is formed. In the end, the final hybrid model is constructed, which contains the encoder part from the *SAE* autoencoder and *LE* layers.

Training data generation

The datasets used in this experiment for training are synthetic. The algorithm for data generation produced *150* thousand scenes with different inclusions such: as circle, square or two them - where each subset contains *50* thousand of one type of samples with noise.

The conductivity of the circle is less, and the conductivity of the square is greater than the background conductivity to obtain similar conditions as in the laboratory where the actual data comes from. Each scene image from the dataset was used in *EIT* simulation to generate potential vectors with lengths equal to *192*.

The synthetic data generation for *EIT* reconstruction was also a difficult (inverse to inverse) problem because the

generated data must be close to real *EIT* data achieved in the laboratory.
In order to gain vectors of potentials based on generated scenes with different kinds of inclusions, the simulation using the finite element method using square shapes was performed.
The simulation algorithm parameters for dataset generation used in the experiments were adapted to get synthetic data close to real data obtained in the laboratory.
Next, the potential differential vectors are computed using received potential vectors:

$$X_i = x_i - x0_i \qquad (1)$$

where:*x* – is the potential vector gained based on the scene containing inclusions, *x0* – is the potential vector gained for the empty scene (with background only),
X – is the potential differential vector, *i* – indicates the position of elements in potential and differential potential vectors.

Obtained samples of reference images (from now on referred to as *Y*) as well as potential differential vectors (after this referred to as *X*) were divided into a training dataset (inclusive *120* thousand samples) and test dataset (inclusive *30* thousand samples).

Preliminary EIT reconstructions using a deterministic algorithm

The preliminary EIT reconstructions using the deterministic algorithm presented below generated *80x80* images based on potential differential vectors from each sample in the training and test datasets. The preliminary reconstructions (based on inputs in the form of potential differential vectors) were done using *Kotre's* regularisation [25] by sensitivity matrix pseudo-inversion:

$$J^{-1} = (J^T J + \lambda R)^{-1} J^T, R = \left(I \cdot (J^T J)\right)^{\frac{1}{2}} \qquad (2)$$

where: J – is the matrix of sensitivity, λ – is the regularisation coefficient established using the gradient method, (·) – is the operator of the multiplication element by element.

Reconstructed conductivity is determined by:

$$\sigma = J^{-1} V \qquad (3)$$

where V – is a final post-processed measurement (in the form of a differential vector).

Preprocessing of data

The data in the experiments was normalised as follows. First, the potential differential vectors are used to compute preliminary *EIT* reconstructions using the deterministic algorithm described earlier. Then, the reference images were normalised to range *<0,1>*. After that, the background pixels have values of *0.5,* while inclusions with conductivity lesser than the background (circles) have values of *0.0* and objects with conductivity greater than the background (squares) have values of *1.0*.
The second stage of reference image processing is the removement of the outer background (caused by the *EIT* simulation program – surrounding electrodes designate the proper EIT area). Since convolutional neural networks consider the entire area of the image, the input and output images should have a consistent background.

The preliminary *EIT* reconstruction images (obtained through a deterministic algorithm) are normalised using the min-max method for each sample (image) separately. This normalisation method was chosen based on our experiments with training EIT reconstruction images autoencoder, and after the data analysis, we noticed that the differences between minimal and maximal values in different images in the entire dataset were too huge. Used min-max normalisation is computed in the preprocessed image in the following way:

$$v_{norm} = \frac{v - v_{min}}{v_{max} - v_{min}} \qquad (4)$$

where: *v* - is the given value from the preliminary *EIT* reconstruction image with preprocessing, v_{min} - is the minimum pixel value in the image, v_{max} - is the maximal pixel value in the image, v_{norm} - is the output pixel value (normalized).

Deep learning correction of *EIT* reconstructions

This section describes research leading to *EIT* reconstruction correction using a modified *UNet* model [26]. Because of the problem of training the classical UNet model, which uses convolutions equal to 3x3, these sizes of convolution filters were changed to 5x5, like in the paper [16]. In addition, the soft sign activation function was set in the model's final layer. The training was done using *120* thousand pairs of images (with preliminary *EIT* reconstructions designated using the deterministic algorithm as input and reference scene images as output). All kinds of images during training (input and output) have 80x80 sizes. We are using *Adam* optimiser in the training process with a learning rate equal to 10^{-4}, *MSE* loss function, and batches with sizes equal to *64* and *45* epochs. After training using the training data set, the following numerical results *MAE* loss and *DICE* metric [27] on training and test datasets were obtained:

Table 1. Obtained results on training and test datasets

DATASET	MAE	DICE
training	0.0017251	97.12
test	0.0031536	92.52

The visual samples of results for three kinds of inclusions inside (circles, squares, circles and squares) are presented in Figure 1.

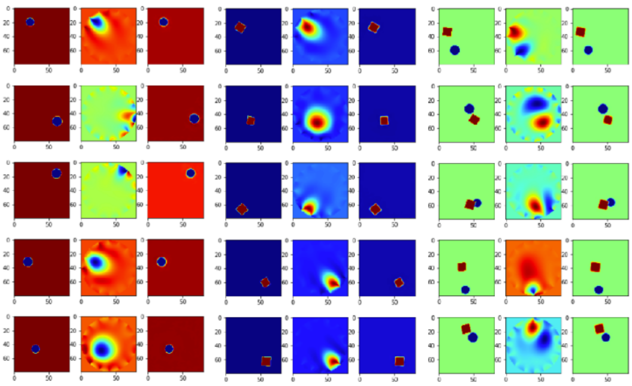

Fig. 1. The sample results of *EIT* reconstructions correction by modified *UNet* model obtained on the test dataset

Testing of modified *UNet* model on the real data

The synthetic data used for modified *UNet* model training was very similar to real data obtained in the laboratory. We have multiple data sets obtained using a custom Electrical Impedance tomograph with two types of inclusions dipped in water. A part of the set only contains a plastic tube (with a circular cross-section), while other sets contain a plastic tube and a metal cuboid block (with a square cross-section). The plastic tube has conductivity smaller than water, while the metal cuboid block has conductivity bigger than water.

For each sample in each real dataset, the potential vectors were obtained. In addition, the potential vectors were also obtained for the case without any inclusion, and potential differential vectors were calculated and saved per each sample (as in the case of synthetic data). After obtaining potential differential vectors, the initial *EIT* reconstructions were performed using a deterministic algorithm (as in the synthetic data case).

Notice that we have only the differential potential vectors obtained for real data. Because we have no reference images, we cannot assess the results numerically. However, all real data sets represent the same scene, and we know the inclusions types and positions to assess the results visually.

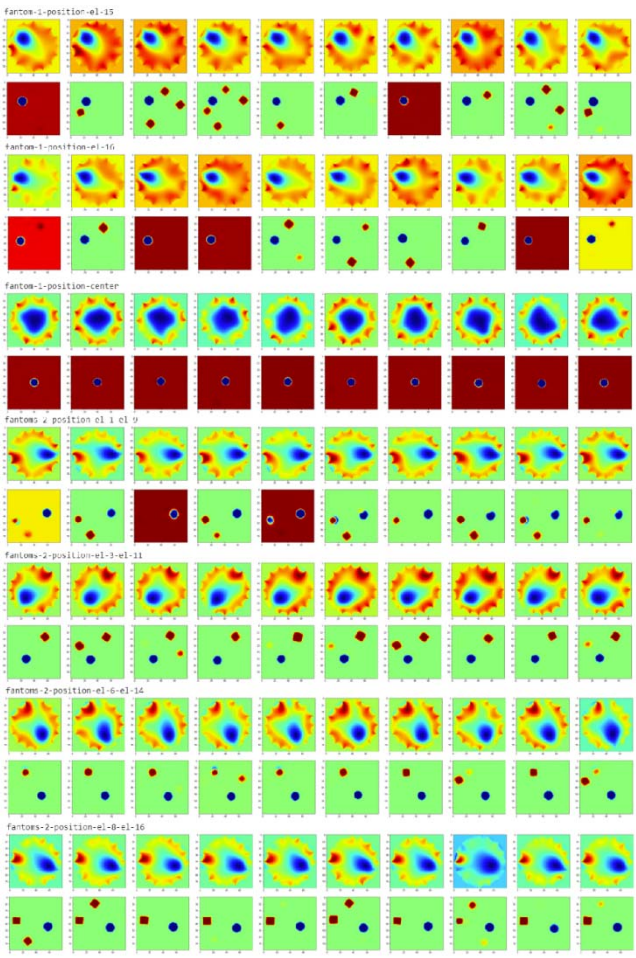

Fig. 2. The sample results of *EIT* reconstructions correction by modified *UNet* model obtained for the real data datasets

Figure 2 shows the sample results of neural corrections of *EIT* reconstructions for part of real data datasets. In one pair of rows, there are *10* sample results obtained per one different real data dataset. Each pair of rows contains initial *EIT* reconstructions (each first row) obtained using a deterministic algorithm and neural correction or *EIT* reconstructions by a modified *UNet* model (each second row). The first three pairs of rows represent datasets with one inclusion (circle), while the next rows represent both inclusions (circles and squares).

After a deep analysis of sample responses, we can conclude that the proper inclusions are in the correct places in the analysed samples, but there are many additional incorrect inclusions.

Because the additional wrong inclusions are in different places and the fact that we have multiple samples representing the same scene in each real data dataset using the simple postprocessing algorithm based on multiple images - network responses, we can eliminate the wrong inclusions. In the beginning, the average of images was calculated:

$$Ipp_{i,j} = I_{k_{i,j}} \tag{5}$$

where: *Ipp* - is the corrected reconstruction image after postprocessing, *I* - is the reconstruction image - *UNet* output for one sample, *k* - is the number of samples, *i, j* - are the coordinates of the image.

After that, the two thresholds are performed to extract inclusions with conductivity smaller than the background and greater than the background separately. Figure 3 shows samples for each dataset after the first (average) and second (thresholding) steps of postprocessing using all samples in the given real data dataset.

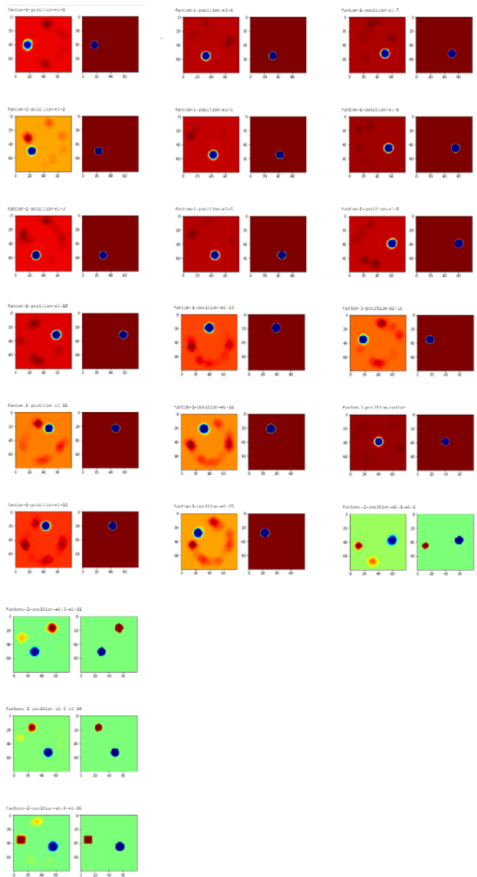

Fig. 3. Results of the first and second stage of the postprocessing algorithm of *UNet* model outputs for each real data dataset comes from the laboratory

Conclusions

This paper used the modified UNet model for successful initial *EIT* reconstruction correction. The initial *EIT* reconstructions were computed using *Kotre's* regularisation using pseudo-inversion of the sensitivity matrix. The method used for initial *EIT* reconstruction works very fast. The modified model after the train was tested on synthetic and real data. After postprocessing outputs for real data, the final results seem to be good.

Autorzy
Łukasz Maciura, Ph.D. Eng., Netrix S.A., Research & Development Centre, Lublin, Poland, e-mail: lukasz.maciura@netrix.com.pl, Tomasz Rymarczyk, Prof. Eng., Netrix S.A., Research & Development Centre, Lublin, Poland, WSEI University, Poland, e-mail: tomasz@rymarczyk.com; Dariusz Wójcik, Ph.D. Eng., Netrix S.A., Research & Development Centre, Lublin, Poland, WSEI University, Poland, e-mail: dariusz.wojcik@netrix.com.pl, Konrad Gauda, Ph.D. Eng., WSEI University, Poland, e-mail: konrad.gauda@wsei.lublin.pl Marcin Kowalski, Ph.D. Eng., WSEI University, Poland, e-mail: marcin.kowalski@wsei.lublin.pl

REFERENCES

[1] Rymarczyk T., Niderla K. Kozłowski E. Król K., Wyrwisz J. Skrzypek-Ahmed S., Gołąbek P., Logistic Regression with Wave Preprocessing to Solve Inverse Problem in Industrial Tomography for Technological Process Control, *Energies*, 14 (2021), No. 23, 8116.
[2] Rymarczyk T., Kłosowski G., Application of neural reconstruction of tomographic images in the problem of reliability of flood protection facilities, *Eksploatacja i Niezawodnosc – Maintenance and Reliability*, 20 (2018); No. 3, 425–434
[3] Kłosowski G., Rymarczyk T., Cieplak T., Niderla K., Skowron Ł., Quality Assessment of the Neural Algorithms on the Example of EIT-UST Hybrid Tomography, *Sensors*, 20 (2020), No. 11, 3324
[4] Koulountzios P., Rymarczyk T., Soleimani M., A triple-modality ultrasound computed tomography based on full-waveform data for industrial processes, *IEEE Sensors* Journal, 21 (2021), No. 18, 20896-20909
[5] Rymarczyk T., Kłosowski G., Hoła A., Sikora J., Wołowiec T., Tchórzewski P., Skowron S., Comparison of Machine Learning Methods in Electrical Tomography for Detecting Moisture in Building Walls, *Energies*, 14 (2021), No. 10, 2777
[6] Kłosowski G., Hoła A., Rymarczyk T., Skowron Ł., Wołowiec T., Kowalski M., The Concept of Using LSTM to Detect Moisture in Brick Walls by Means of Electrical Impedance Tomography, *Energies*, 14 (2021), No. 22, 7617
[7] Kłosowski G., Rymarczyk T., Kania K., Świć A., Cieplak T., Maintenance of industrial reactors supported by deep learning driven ultrasound tomography, *Eksploatacja i Niezawodnosc – Maintenance and Reliability*; 22 (2020), No 1, 138–147
[8] Styła, M., Adamkiewicz, P., Optimisation of commercial building management processes using user behaviour analysis systems supported by computational intelligence and RTI, *Informatyka, Automatyka, Pomiary W Gospodarce I Ochronie Środowiska*, 12 (2022), No 1, 28-35
[9] Łukiański, M., & Wajman, R., The diagnostic of two-phase separation process using digital image segmentation algorithms, *Informatyka, Automatyka, Pomiary w Gospodarce i Ochronie Środowiska*, (2020),. 10(3), 5-8
[10] Korzeniewska, E., Sekulska-Nalewajko, J., Gocawski, J., Drożdż, T., Kiebasa, P., Analysis of changes in fruit tissue after the pulsed electric field treatment using optical coherence tomography, *EPJ Applied Physics*, 91 (2020), No. 3, 30902
[11] Korzeniewska, E., Krawczyk, A., Mróz, J., Wyszyńska, E., Zawiślak, R., Applications of smart textiles in post-stroke rehabilitation, *Sensors*, 20 (2020), No. 8, 2370.
[12] Rybak G., Strzecha K., Short-Time Fourier Transform Based on Metaprogramming and the Stockham Optimization Method, *Sensors*, 21 (2021), No. 12, 4123
[13] Mosorov V.; Rybak G., Sankowski D., Plug Regime Flow Velocity Measurement Problem Based on Correlability Notion and Twin Plane Electrical Capacitance Tomography: Use Case, *Sensors*, 21 (2021), No. 6, 2189
[14] Dušek J., Hladký D., Mikulka J., Electrical Impedance Tomography Methods and Algorithms Processed with a GPU, *In PIERS Proceedings*, (2017), 1710-1714
[15] Shi, XW; Tan, C; Dong, F; dos Santos, EN; da Silva, MJ, Conductance Sensors for Multiphase Flow Measurement: A Review, *IEEE Sensors Journal*, 21 (2021), No. 11, 12913-12925
[16] Hamilton S. J., Hauptmann A., Deep D-bar: Real time Electrical Impedance Tomography Imaging with Deep Neural Networks, *IEEE Transactions on Medical Imaging*, 37 (2018), No. 10, 2367-2377
[17] Klosowski G., Rymarczyk T., Using neural networks and deep learning algorithms in electrical impedance tomography, *Informatyka Automatyka Pomiary w Gospodarce I Ochronie Środowiska*, 7 (2017), No. 3, 99-102
[18] Malone E., Gustavo Sato dos Santos, David Holder and Simon Arridge, A Reconstruction-Classification Method for Multifrequency Electrical Impedance Tomography, *IEEE Transactions on Medical Imaging*, 34 (2015), No 7, 1486 - 1497
[19] Khan T. A., Ling S.H., Review on Electrical Impedance Tomography: Artificial Intelligence Methods and its Applications, *Algorithms*, 12 (2019), No. 5, 88
[20] Seo J. K., Kim K.C., Jargal A., Lee K., Harrach B., Learning-Based Method for Solving Ill-Posed Nonlinear Inverse Problems: A Simulation Study of Lung EIT, *SIAM J. Imaging Sci.*, 12 (2019), No. 3, 1275-1295
[21] Fernandez-Fuentes X., Mera D., Gomez A., Vidal-Franco I., Towards a Fast and Accurate EIT Inverse Problem Solver: A Machine Learning Approach, *Electronics*, 7 (2018), No. 12, 422
[22] Li X., Lu Y., Wang J., Dang X., Wang Q., Duan X., An image reconstruction framework based on deep neural network for electrical impedance tomography, *IEEE International Conference on Image Processing (ICIP)*, 2017, 3585–3589
[23] Li. X., Zhou Y., Wang Y., Wang Q., Lu Y., Duan X., Sun Y., Zhang J., Liu Z., A novel deep neural network method for electrical impedance tomography, *Transactions of the Institute of Measurement and Control*, 41 (2019), No. 14, https://doi.org/10.1177/0142331219845037
[24] Hamilton S. J., Mueller J. L., Santos T. R., Robust computation in 2D absolute EIT (a-EIT) using D-bar methods with the' exp' approximation, *Physiological Measurement*, 39 (2018), No. 6, 064005
[25] Kotre C. J., A sensitivity coefficient method for the reconstruction of electrical impedance tomograms, *Clin Phys Physion Meas.*, 10 (1989), No. 3, 275-81
[26] Ronneberger O., Fischer P., Brox T., U-Net: Convolutional Networks for Biomedical Image Segmentation, *Medical Image Computing and Computer – Assisted Intervention*, 9351 (2015), 234 - 241
[27] Aziz Taha A., Hanbury A., Metrics for evaluating 3D medical image segmentation: analysis, selection, and tool, *BMC Medical Imaging*, 15 (2015), No. 29, 1-28